Computers, Materials & Continua

Tech Science Press

https://doi.org/10.32604/cmc.2026.082702

ARTICLE

Spontaneous 2D Film Formation of Alkanes on Isoelectronic Substrates: BN Nanosheet vs. Graphene. Quantum Chemical Semi-Empirical Approach

Elena S. Kartashynska*

Department of Supramolecular Chemistry, L.M. Litvinenko Institute of Physical Organic and Coal Chemistry, Donetsk, Russia

*Corresponding Author: Elena S. Kartashynska. Email: elenafomina-ne@yandex.ru

Received: 20 March 2026; Accepted: 23 June 2026; Published: 13 August 2026

ABSTRACT: The discovery of graphene and its unique physicochemical properties has catalyzed intensive research into alternative two-dimensional (2D) materials, with a view to their prospective applications in diverse fields of physics, chemistry, and materials science. In this context, there is a notable scientific interest in developing computationally efficient theoretical approaches capable of reliably estimating key parameters of organic films deposited on 2D surfaces. This objective necessitates a rigorous selection and validation of appropriate computational methods, ensuring an optimal balance between computational cost and predictive accuracy. This study presents a method for evaluating the thermodynamic and structural characteristics of alkane monolayers on the surfaces of 2D materials: graphene and boron nitride nanosheet (BNNS). The proposed approach employs the semi-empirical PM6 method, supplemented with corrections for dispersion interactions and hydrogen bonds. This enables the calculation of large alkane aggregates interacting with surface model molecules (tricircumcoronene $C_{150}H_{30}$ for graphene and $B_{75}N_{75}H_{30}$ for BNNS), allowing identification of the key interaction increments that govern monolayer formation. The calculations demonstrate that the D3H4 correction is required for an accurate description of C–H$\cdots\pi$ interactions during alkane adsorption on BNNS surfaces, whereas the DH2 correction suffices for similar interactions on graphene-like surfaces. The evaluated interaction increments reveal that C–H$\cdots\pi$ interactions are less advantageous on BNNS compared to graphene. However, unfavorable type of C–H$\cdots$H–C interactions between alkane molecules counterbalance the favorable C–H$\cdots\pi$ ones, setting a threshold chain length for alkanes capable of forming crystalline films on these surfaces. According to the results, alkanes with 14 carbon atoms in the chain can spontaneously form 2D films on BNNS at standard temperature. It is one carbon atom longer than on graphene. Two packing arrangements in 2D monolayers: “straight” and “herringbone”, are analyzed. They exhibit similar clusterization Gibbs energies, with a slight disadvantage for the “herringbone” arrangement in longer-chain alkanes at standard temperature. The presence of the “herringbone” 2D structure may represent a pre-melting solid-solid phase transition, accounting for a 1.9 K difference in melting temperature, as confirmed by experimental data.

KEYWORDS: Monomolecular films; alkanes; graphene; boron nitride nanosheet; thermodynamics

1 Introduction

The study of the adsorption properties of various materials in relation to alkanes and their functional substitutes is relevant both from a theoretical and practical point of view. Pilot works in the middle of the last century on the experimental assessment of the adsorption heats of alkanes [1] and alkanols [2] on graphite were subsequently supplemented by numerous results concerning the structure of the resulting mono- and multilayers using AFM and STM methods [3–5], X-ray diffraction analysis [6], differential scanning calorimetry [7]. The spectrum of the surfactants studied has also been significantly expanded [5].

Research priorities in this field shifted at the dawn of the 21st century towards 2D graphite analogues, a development catalyzed by the emergence of graphene as the first and most prominent example [8]. Graphite may be considered as an ordered assembly of parallel-stacked graphene layers interconnected exclusively via van der Waals interactions. They determine the differences in properties for graphite and its 2D analogue. The recent advances in exfoliation methodologies have significantly intensified scientific interest in the investigation of 2D nanostructures. This interest is primarily driven by the pronounced influence of surface and interface effects, which become particularly dominant at the nanoscale and manifest most prominently in low-dimensional systems.

The well-documented and extensively publicized exceptional properties of graphene [9,10] have catalyzed significant interest in the exploration of alternative 2D materials derived from elements of the IIIA and VA groups of the periodic table. A prominent example is hexagonal boron nitride nanosheet (BNNS) [11], which possesses an isoelectronic structure relative to graphene, demonstrates high chemical and thermal stability, and, in contrast to graphene, displays dielectric behavior. Concurrent efforts to synthesize additional 2D materials exhibiting either analogous or divergent electronic structures—such as GaN, BAs, and MgO—have generated substantial theoretical interest in elucidating the molecular-scale behavior of alkanes and other organic compounds upon these surfaces [12]. This line of inquiry is particularly pertinent to the development of advanced sensor and catalytic systems [13,14], as well as to the systematic investigation of the adsorptive characteristics of these novel 2D surfaces.

The development of advanced computational methods, such as molecular dynamics modeling [15], DFT [16–18], and semi-empirical quantum chemical approaches [19,20], has significantly enhanced the ability to reveal the structural characteristics of alkane monolayers and their derivatives. These methods also allow for a quantitative evaluation of how various intermolecular interactions influence the thermodynamic parameters of adsorption and film formation processes. Notably, the dispersion-corrected semi-empirical PM6 method has proven effective in describing the film formation of *n*-alkanes and *n*-alkanols on graphene surfaces [19,20]. Complementing this, a substantial array of experimental data exists on the adsorption heats and melting points of 2D alkane crystalline monolayers deposited on graphite and hBN substrates [15,21,22]. This combination of theoretical and experimental insights facilitates the further use of the PM6 method, particularly in assessing hBN nanosheet potential as an adsorbent and in modeling the temperature dependent conditions for the spontaneous formation of C_nH_{2n+2} alkane crystalline monolayers (n = 2–16) on isoelectronic surfaces.

2 Calculation Scheme and Methods

To model the surfaces of graphene and boron nitride 2D sheet, polyaromatic molecular systems were employed: tricircumcoronene ($C_{150}H_{30}$) for graphene and its structural analogue $B_{75}N_{75}H_{30}$ for BNNS (Fig. 1). This choice aligns with established practices in computational studies [16,23–26], where polyaromatic systems serve as finite-cluster models for assessing thermodynamic parameters of molecular interactions with carbon-based surfaces. Such models are routinely used to study: interactions of small molecules (H_2, N_2, He, H_2O, C_2H_2, C_2H_5OH, etc.) with carbon surfaces; physisorption of noble gases on hBN [27]; adsorption of larger molecules on hexagonal boron nitride [28,29].

Notably, the use of finite single-layer models with hydrogen-terminated edges as in Ref. [27] has been validated in studies of heterocycle adsorption on B/N/BN-doped graphene [30]. These works demonstrated that even a coronene molecule ($C_{24}H_{12}$) can adequately represent a doped graphene surface for adsorption studies, with larger systems ($C_{42}H_{16}$–$C_{66}H_{20}$) confirming this conclusion. Building on this foundation, previous studies [19,20] established that tricircumcoronene (with 51 condensed aromatic rings) provides

sufficient lateral dimensions to orient alkanes up to tetradecane. This justifies its use, as well as its BNNS analogue, in simulating alkane adsorption and clusterization processes.

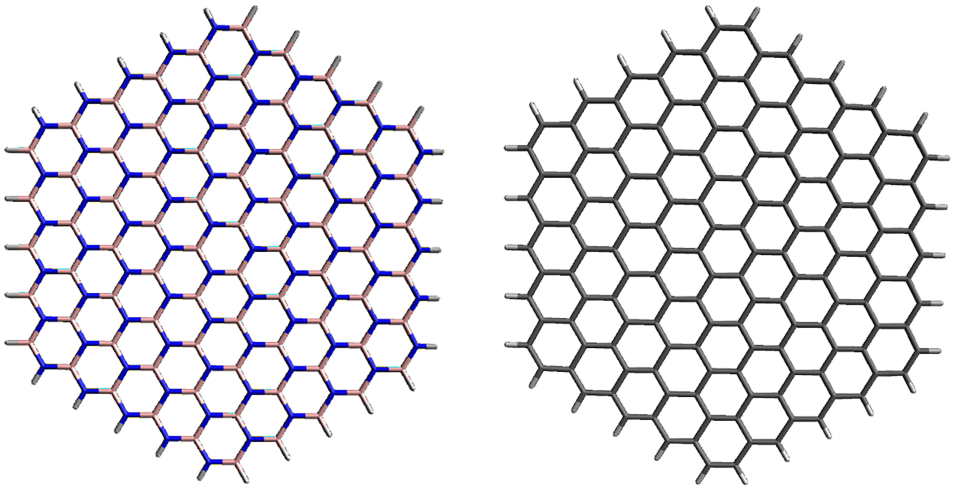

Figure 1: Optimized geometric structure of $B_{75}N_{75}H_{30}$ and $C_{150}H_{30}$ within PM6-D3H4 and PM6-DH2 method correspondingly (C is dark grey, H is light grey, N is blue, B is light pink).

Alkane molecules can adopt two orientations on the regarded surfaces: parallel or perpendicular depending on the alignment of the alkane chain C–C–C "zigzag" plane relative to the graphene or BNNS sheet. Computational studies [3,31] show that alkanes preferentially adsorb in a parallel orientation on graphite (graphene) surfaces. This trend is also observed for hexagonal boron nitride: Ref. [15] confirms that alkanes from ethane to octane adsorb more favorably in a parallel configuration on BNNS, as demonstrated by molecular modeling with a universal force field.

The strategy for calculation of the thermodynamic parameters of alkane film formation as well as their derivatives on flat surfaces includes the following main steps:

(1) Construction of complexes alkane–model surface molecule (tricircumcoronene $C_{150}H_{30}$ and $B_{75}N_{75}H_{30}$ for graphene and BNNS, respectively), where alkane molecules adopt the most elongated all-*trans* conformation according to STM data [32,33].

(2) Calculation of thermodynamic parameters of binding for homologous series of alkanes and the model surface molecule. The enthalpy and entropy of binding are calculated using the expressions:

$$\Delta H_T^{bind} = \Delta_f H^0_{T,complex} - \Delta_f H^0_{T,surf.mol.} - \Delta_f H^0_{T,HC}, \quad (1)$$

$$\Delta S_T^{bind} = S^0_{T,complex} - S^0_{T,surf.mol.} - S^0_{T,HC}, \quad (2)$$

where $\Delta_f H^0_{T,complex}$ and $S^0_{T,complex}$ are the enthalpy and absolute entropy of intermolecular complex formation (T = 298 K), $\Delta_f H^0_{T,surf.mol.}$, $S^0_{T,surf.mol.}$ and $\Delta_f H^0_{T,HC}$, $S^0_{T,HC}$ are the enthalpies and absolute entropies of formation of the model surface molecule and alkane correspondingly.
The free binding energy is calculated as:

$$\Delta G_T^{bind} = \Delta H_T^{bind} - T\Delta S_T^{bind}. \quad (3)$$

(3) Quantifying the contribution of C–H$\cdots\pi$ interactions to the formation of complexes alkane–model surface molecule

(4) Calculation of thermodynamic parameters characterizing alkane interactions during monolayer growth in two propagation directions, using the following formulas:

$$\Delta H_T^{Cl} = \Delta_f H_{T,m}^0 - m \cdot \Delta_f H_{T,HC}^0, \quad (4)$$

$$\Delta S_T^{Cl} = \Delta_f S_{T,m}^0 - m \cdot \Delta_f S_{T,HC}^0. \quad (5)$$

Here $\Delta_f H_{T,m}^0$ and $S_{T,m}^0$ denote the formation enthalpy and absolute entropy of alkane aggregates at temperature T with m indicating the number of alkane molecules in the associate (for example, $m = 2$ in case of dimers).

(5) The use of the principle of pair additivity for alkane–adsorbent and alkane–alkane interactions. It enables the construction of a scheme for the thermodynamic parameters of film formation, which incorporates C–H$\cdots\pi$ interactions, CH$\cdots$HC interactions, and the contributions of terminal CH_3 fragments, evaluated for both propagation directions of the monolayer per alkane molecule within the 2D layer.

In a pioneering study, Vysotsky et al. [34] proposed the concept of additive energy variation for attaching fatty alcohol molecules to clusters, later refined and summarized in Ref. [35] for multiple surfactant classes, while neglecting cooperative effects important in H-bonded systems. It is acceptable assuming that the liquid expanded to liquid condensed phase transition in studied monolayers goes via dimer or trimer aggregation and their subsequent enlargement up to 2D film. This simplified approach proved effective, allowing prediction of the minimum chain length needed for spontaneous monolayer formation at the air/water interface (consistent with experiments); chain length dependence of surface pK_a values for carboxylic acids, and other experimentally verified trends.

(6) Analysis of geometric parameters of the monolayer unit cells.

(7) Establishing the relationship between the crystallization/melting temperature of alkane monolayers and hydrocarbon chain length using expressions for enthalpy and entropy of the film formation per molecule. Calculations are performed using schemes of varying theoretical validity. Comparison with experimental data.

Geometric optimization of individual molecules and molecular complexes, along with thermodynamic parameter calculations, was carried out using the MOPAC2016 software package [36]. The semi-empirical quantum chemical PM6 method, supplemented with DH2 and D3H4 dispersion and hydrogen-bonding corrections, was employed for these calculations. The thermodynamic parameters of alkane film formation on the graphene surface are estimated using the PM6-DH2 method. The results obtained in Ref. [19] indicate an adequate reproduction of the threshold chain length of alkanes capable of film formation on the graphene surface at the standard temperature. In this case, the Gibbs energy serves as the stability criterion for the calculated alkane–$C_{150}H_{30}$ complexes, in contrast to many works that limit themselves to estimating only the heat or enthalpy of adsorption, or the interaction energy in the complex (for example, in the Ref. [17]). However, D3H4 correction for PM6 method is required for consideration alkane–$B_{75}N_{75}H_{30}$ complexes, unlike alkane–$C_{150}H_{30}$ systems. Additionally, density functional theory calculations were performed using the ORCA software package (version 5.0.4) [37]. The hybrid B3LYP-D3 functional and the 6-311G** basis set were employed for small complexes: borazole–methane, benzene–methane, coronene and $B_{12}N_{12}H_{12}$with alkanes from ethane to butane. Basis set superposition error (BSSE) correction was applied via the counterpoise method according to Boys and Bernardi [38].

3 Results and Discussion

3.1 Interactions in the Borazole–Methane and Benzene–Methane Systems

To verify the semi-empirical PM6 method (including various corrections for dispersion interactions and hydrogen bonds), the geometrical parameters of the borazole molecule ($B_3N_3H_6$) as a structural unit of the 2D hBN plane were calculated. The results for bond lengths (B–N, N–H, and B–H), dipole moment, and polarizability are presented in Table S1 of the Supplementary Materials. The data show that the PM6 method with DH2 and D3H4 corrections yields nearly identical values for these parameters, which closely match the results from Ref. [39] except for the polarizability of $B_3N_3H_6$. The semi-empirical estimate of polarizability is approximately 15% lower than the values obtained from DFT calculations using the B3LYP and CAM-B3LYP functionals within the 6-31+G** and 6-31++G** basis sets. Furthermore, the dipole moment of the borazole molecule calculated via the PM6 method is roughly two orders of magnitude lower than the DFT results reported in study [39], and is effectively zero. This finding aligns with available experimental data [40]. It is also noteworthy that the D3H4 correction combined with the PM6 method significantly underestimates the heats of formation for alkanes. Table S2 of the Supplementary Materials compares the calculated and experimental values of $\Delta_f H^0_{298}$ and S^0_{298} for all compounds considered in this work. Despite this limitation, subsequent sections will demonstrate that the PM6-D3H4 approach is nevertheless adequate for describing intermolecular interactions in the alkane–BNNS system.

The satisfactory agreement between semi-empirical calculations of the borazole structure and higher-level theoretical data justifies proceeding to the calculation of simple borazole–methane complexes. Fig. 2 illustrates the structures of these small complexes, alongside benzene–methane complexes for comparison. All presented associates were optimized using the PM6 method with DH2 and D3H4 corrections, as well as density functional theory at the B3LYP-D3/6-311G** level. This dual approach enables a preliminary evaluation of the semi-empirical method's adequacy (and the effectiveness of the corresponding corrections) for describing intermolecular interactions in larger alkane–BNNS systems discussed later in the work. The choice of the structures of benzene–methane complexes shown in Fig. 2 is due to the fact that they are among the most energetically advantageous according to the literature data [41,42]. Borazole–methane complexes similar to them are considered in order to assess the relative energy preference of C–H$\cdots\pi$ interactions realized in isoelectronic structures.

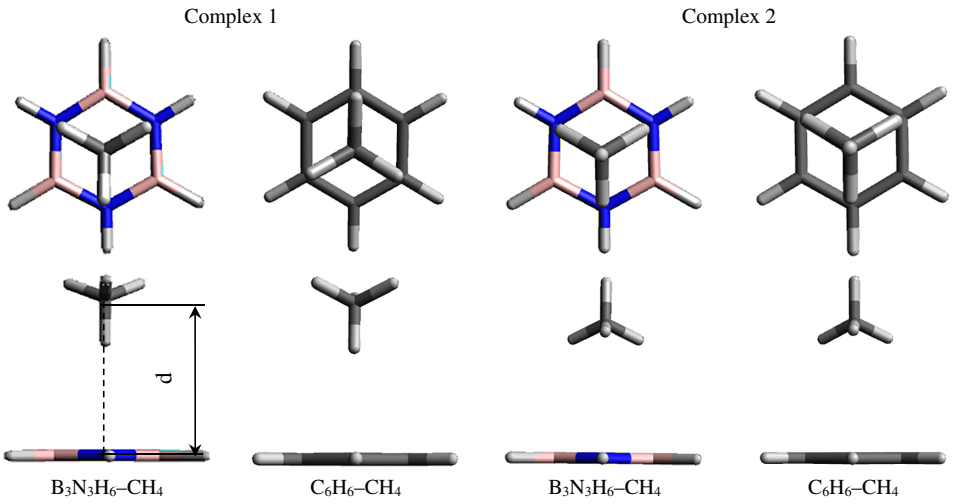

Figure 2: Optimized geometric structure of borazole–methane and benzene–methane complexes (B3LYP-D3/6-311G** level of theory).

The computational results reveal some differences in the accuracy of the semi-empirical PM6 method for benzene–methane vs. borazole–methane complexes. The distance from the methane carbon atom to the center of the benzene ring $d(C\cdots C_6H_6)$ in complex 1, estimated using the semi-empirical PM6 method, is (0.11–0.20) Å shorter than that obtained at the B3LYP-D3/6-311G** level of theory (see Table 1). The experimentally recorded value of $d(C\cdots C_6H_6)$ is 3.8 Å [24]. In contrast, for structurally similar borazole–methane complexes, the distance $d(C\cdots B_3N_3H_6)$ estimated by the PM6-D3H4 method shows excellent agreement with DFT calculations. The experimentally found value of $d(C\cdots C_6H_6)$ is 3.6 Å for complex 2 of benzene with methane [43], which is accurately reproduced by DFT. The semi-empirical approach underestimates this distance by (0.15–0.17) Å. Particularly, DFT calculations across a wide range of functionals (reported in Ref. [23]) estimate this distance within the range of (3.46–3.79) Å using a very representative number of functionals given in the study [23].

Table 1: Calculated thermodynamic and structural data for borazole–methane and benzene–methane complexes.

Method	ΔH^{bind}_{298}, kJ/mol		ΔS^{bind}_{298}, J/(mol·K)		ΔG^{bind}_{298}, kJ/mol		Distance *d*, Å	
	C_6H_6–CH_4	$B_3N_3H_6$–CH_4	C_6H_6–CH_4	$B_3N_3H_6$–CH_4	C_6H_6–CH_4	$B_3N_3H_6$–CH_4	C⋯ C_6H_6	C⋯ $B_3N_3H_6$
Complex 1								
PM6-DH2	−6.29	−5.21*	−26.06	−53.76*	1.47	10.81*	3.55	3.66
PM6-D3H4	−6.43	−5.12*	−42.55	−38.97*	6.25	6.49*	3.64	3.83
B3LYP-D3/6-311G**	−8.34	−7.01	−31.67	−40.04	1.10	4.92	3.75	3.87
Complex 2								
PM6-DH2	−6.05	−7.48	−69.79	−48.59	14.75	7.00	3.43	3.43
PM6-D3H4	−6.88	−7.14	−73.36	−75.38	14.98	15.32	3.41	3.42
B3LYP-D3/6-311G**	−7.62	−7.58	−38.20	−26.98	3.76	0.46	3.58	3.54

Note: *methane molecule in $B_3N_3H_6$–CH_4 complex 1 was "frozen" because this structure transformed into complex 2 during optimization procedure in *PM*6 with both corrections DH2 and D3H4.

From the Gibbs binding energy, it can be seen that all the considered complexes are unstable at the standard temperature. However, it is possible to compare the values of ΔG^{bind}_{298} for them. The borazole–methane complex 1 is less energetically preferable than the similar structure of the benzene–methane complex. Semi-empirical optimization of borazole–methane complex 1 leads to its transformation into the more energetically favorable complex 2. To calculate the thermodynamic parameters of complex 1 formation, the coordinates of the methane molecule in the $B_3N_3H_6$–CH_4 system were therefore 'frozen' during the calculation. The data shown in Table 1 indicate a greater adequacy of the PM6-D3H4 method in estimating the value of ΔG^{bind}_{298} for complex 1 of $B_3N_3H_6$–CH_4 and, conversely, the PM6-DH2 method for C_6H_6–CH_4 complex 1. Consideration of this particular structure of the C_6H_6–CH_4 and $B_3N_3H_6$–CH_4 complexes, where one hydrogen atom of methane interacts with benzene or borazole, is important because the parallel orientation of long-chain homologues on the surface of graphene or BNNS results in C–H$\cdots\pi$ interactions between one hydrogen of each methylene fragment of alkane and one π-electronic system of the adsorbent.

The enthalpy component of one C–H$\cdots\pi$ interaction for the complex 1 of $B_3N_3H_6$–CH_4 is approximately 1 kJ/mol lower (in absolute value) than for C_6H_6–CH_4, when estimated using the PM6 method with both

corrections, as well as in the DFT calculation. The experimentally determined dissociation energy for the methane–benzene complex is (4.3–4.7) kJ/mol [44], consistent with prior estimates of C–H$\cdots\pi$ interaction energies (4.4–8.0) kJ/mol reported in Refs. [23,45,46]. For the $B_3N_3H_6$–CH_4 system, however, no equivalent theoretical or experimental data are available in the literature for comparison. The calculated values of ΔH_{298}^{bind} in the C_6H_6–CH_4 complex correlate with the values of the contributions of the C–H$\cdots\pi$ interactions of the considered structure to the adsorption heats of alkanes on the surface of highly oriented pyrolytic graphite 7.53 kJ/mol. While the corresponding contribution of C–H$\cdots\pi$ interactions to the adsorption heats of alkanes on hBN was lower and amounted to 5.60 kJ/mol [15]. Given the strong alignment of results with both experimental measurements and higher-level theoretical calculations, the PM6-D3H4 method is recommended for future studies of alkane–BNNS systems. Specifically, the inclusion of the D3H4 correction enhances the accuracy of the method, providing outcomes that are consistent in both qualitative and quantitative terms.

In Ref. [19], the influence of polyaromatic hydrocarbon molecule size used to model the graphene surface on the thermodynamic parameters of methane binding was investigated using the PM6-DH2 method. The calculations revealed that, starting from tricircumcoronene ($C_{54}H_{18}$), the thermodynamic parameters of methane binding are nearly identical to those obtained for larger polyaromatic hydrocarbons(PAHs) such as di-($C_{96}H_{24}$) and tricircumcoronene ($C_{150}H_{30}$). Complementary findings were reported by Smith and Patkowski [24], who studied methane interactions with graphene-like surfaces using the B3LYP functional with D3 dispersion correction and other benchmark methods. They demonstrated that extending the PAH beyond circumcoronene induces only a minor change in interaction energy. This justifies the use of circumcoronene as a sufficient model for graphene surfaces, provided that the PAH diameter exceeds the alkane molecule length by two rings of condensed nuclei; this condition minimizes the influence of terminal hydrogen atoms on the calculated parameters. The diameter of tricircumcoronene ($C_{150}H_{30}$) meets this requirement for studying alkane binding up to decane. However, complexes involving longer-chain alkanes need additional optimization procedures. A similar approach was applied to evaluate the thermodynamic parameters of alkane binding to $B_{75}N_{75}H_{30}$.

The use of finite surface models enables precise differentiation of interaction contributions between alkane fragments (methyl and methylene groups) and the condensed nuclei of the model molecules $C_{150}H_{30}$ and $B_{75}N_{75}H_{30}$. Importantly, these interaction patterns remain consistent even for larger surface fragments. Thermodynamic binding data for alkanes with chain lengths of 2–14 carbon atoms, as reported in the subsequent section, provide sufficient information to establish a regression relationship between binding parameters and alkane chain length. Consequently, there is no necessity to increase the size of the surface-modeling molecule when calculating larger alkane complexes or their associates. This approach offers significant computational advantages. It substantially reduces calculation time, even when using semi-empirical methods. The benefits become even more pronounced when employing DFT methods. As demonstrated in study [16], DFT calculations require approximately 1000 times more computational time than PM6 calculations, yet they yield a comparable level of accuracy in estimating interaction energies for small molecule complexes on PAH models of graphene surfaces.

3.2 Assessment of Alkane (n = 2–14) Interactions with $B_{75}N_{75}H_{30}$

Fig. 3 presents the optimized structures of alkane complexes formed on the surfaces of hexagonal $B_{75}N_{75}H_{30}$ and tricircumcoronene, using decane as an illustrative example. In these structures, the alkane molecule adopts a “linear” conformation and lies parallel to the adsorbent surface. Conversely, a perpendicular orientation of the alkane carbon chain relative to the adsorbent plane is energetically less favorable [19] and is practically not observed under standard temperature conditions. Enthalpy, entropy, and Gibbs energy

of formation and binding were calculated for C_2–C_{14} alkane complexes with model adsorbents ($B_{75}N_{75}H_{30}$, $C_{150}H_{30}$) using the PM6 method (without correction, with DH2, and with D3H4 corrections for dispersion interactions and hydrogen bonds). This approach helps assess the suitability of each correction for the studied systems. Results are presented in Table 2.

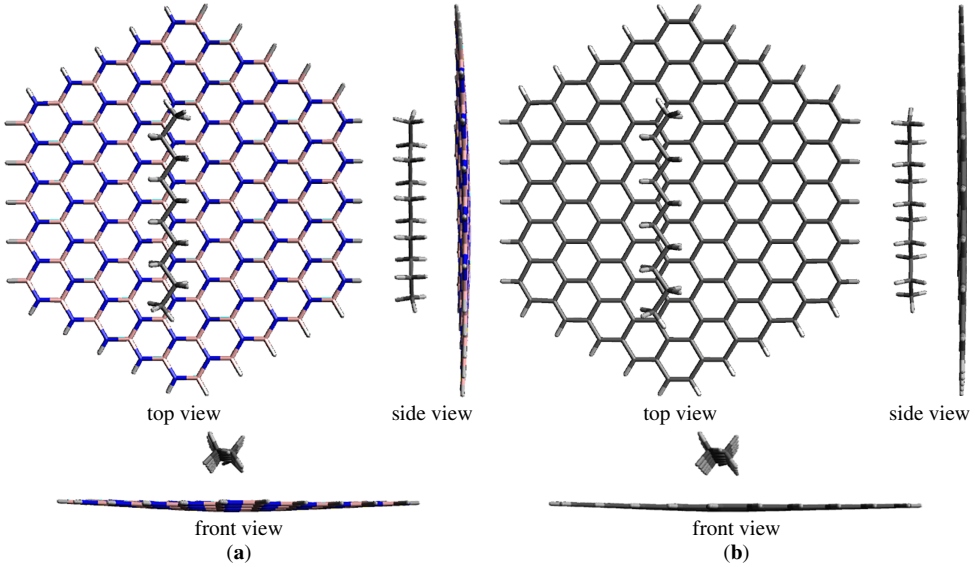

Figure 3: Optimized structures of decane–$B_{75}N_{75}H_{30}$ complexes (**a**) and decane–$C_{150}H_{30}$ (**b**) in PM6-D3H4 and PM6-DH2 method correspondingly.

Table 2: Thermodynamic parameters of binding for alkane–$C_{150}H_{30}$ and alkane–$B_{75}N_{75}H_{30}$ complexes in PM6 method.

Alkane–Surface	Parameters of Complex Binding									Q_{ads}, kJ/mol [15,47]
	ΔH^{bind}_{298}, kJ/mol	ΔS^{bind}_{298}, J/(mol·K)	ΔG^{bind}_{298}, kJ/mol	ΔH^{bind}_{298}, kJ/mol	ΔS^{bind}_{298}, J/(mol·K)	ΔG^{bind}_{298}, kJ/mol	ΔH^{bind}_{298}, kJ/mol	ΔS^{bind}_{298}, J/(mol·K)	ΔG^{bind}_{298}, kJ/mol	
Graphene ($C_{150}H_{30}$)		PM6			PM6-DH2			PM6-D3H4		
C_2H_6–$C_{150}H_{30}$	−2.64	−51.99	12.86	−22.81	−88.21	3.47	−20.30	−50.33	−5.30	20.08
C_3H_{16}–$C_{150}H_{30}$	−3.95	−81.44	20.32	−30.05	−107.23	1.90	−27.76	−67.80	−7.55	27.45
C_4H_{10}–$C_{150}H_{30}$	−5.82	−88.35	20.51	−37.42	−118.39	−2.14	−35.78	−76.02	−13.12	34.43
C_5H_{12}–$C_{150}H_{30}$	−7.15	−99.50	22.50	−45.11	−129.37	−6.56	−43.97	−90.35	−17.04	41.71
C_6H_{14}–$C_{150}H_{30}$	−8.46	−109.33	24.12	−52.64	−140.55	−10.76	−51.75	−111.30	−18.58	49.62
C_7H_{16}–$C_{150}H_{30}$	−9.74	−119.43	25.85	−60.57	−149.80	−15.93	−59.58	−113.86	−25.64	–
C_8H_{18}–$C_{150}H_{30}$	−11.07	−129.62	27.56	−68.52	−161.08	−20.52	−67.39	−129.91	−28.67	–
C_9H_{20}–$C_{150}H_{30}$	−12.38	−138.25	28.82	−76.45	−180.82	−22.56	−75.17	−139.10	−33.71	–
$C_{10}H_{22}$–$C_{150}H_{30}$	−13.70	−148.77	30.63	−84.24	−183.57	−29.53	−82.92	−156.91	−36.16	–
$C_{11}H_{24}$–$C_{150}H_{30}$	−15.01	−166.19	34.52	−92.01	−215.90	−27.67	−90.58	−170.91	−39.64	–
$C_{12}H_{26}$–$C_{150}H_{30}$	−16.20	−170.95	34.74	−99.34	−228.28	−31.31	−97.79	−171.61	−46.65	–
$C_{13}H_{28}$–$C_{150}H_{30}$	−17.37	−189.70	39.16	−106.64	−247.08	−33.01	−104.92	−181.63	−50.80	–
$C_{14}H_{30}$–$C_{150}H_{30}$	−18.48	−200.58	41.29	−113.06	−244.52	−40.19	−112.08	−173.75	−60.30	–
BNNS ($B_{75}N_{75}H_{30}$)		PM6			PM6-DH2			PM6-D3H4		
C_2H_6–$B_{75}N_{75}H_{30}$	−1.06	−30.93	8.16	−20.99	−55.45	−4.46	−17.05	−54.48	−0.81	20.48
C_3H_{16}–$B_{75}N_{75}H_{30}$	−1.22	−40.19	10.76	−30.37	−74.57	−8.15	−22.72	−58.07	−5.42	26.24
C_4H_{10}–$B_{75}N_{75}H_{30}$	−1.61	−53.37	14.30	−36.81	−92.30	−9.30	−29.28	−74.86	−6.97	32.46
C_5H_{12}–$B_{75}N_{75}H_{30}$	−1.99	−65.40	17.50	−46.92	−113.14	−13.21	−35.87	−84.91	−10.57	38.20
C_6H_{14}–$B_{75}N_{75}H_{30}$	−2.37	−73.82	19.63	−55.12	−126.42	−17.45	−42.33	−101.47	−12.10	43.87

(Continued)

Table 2 (continued)

Alkane–Surface	Parameters of Complex Binding									Q_{ads}, kJ/mol [15,47]
	ΔH_{298}^{bind}, kJ/mol	ΔS_{298}^{bind}, J/(mol·K)	ΔG_{298}^{bind}, kJ/mol	ΔH_{298}^{bind}, kJ/mol	ΔS_{298}^{bind}, J/(mol·K)	ΔG_{298}^{bind}, kJ/mol	ΔH_{298}^{bind}, kJ/mol	ΔS_{298}^{bind}, J/(mol·K)	ΔG_{298}^{bind}, kJ/mol	
C_7H_{16}–$B_{75}N_{75}H_{30}$	−2.74	−83.33	22.09	−63.34	−135.11	−23.08	−48.69	−111.67	−15.41	46.15
C_8H_{18}–$B_{75}N_{75}H_{30}$	−3.15	−89.09	23.40	−71.30	−137.31	−30.38	−55.15	−125.52	−17.75	52.34
C_9H_{20}–$B_{75}N_{75}H_{30}$	−3.55	−91.37	23.68	−79.30	−147.93	−35.22	−61.63	−141.41	−19.49	–
$C_{10}H_{22}$–$B_{75}N_{75}H_{30}$	−3.95	−103.09	26.77	−87.14	−160.37	−39.35	−67.78	−146.97	−23.98	–
$C_{11}H_{24}$–$B_{75}N_{75}H_{30}$	−4.36	−131.20	34.73	−94.94	−187.35	−39.11	−73.92	−161.74	−25.73	–
$C_{12}H_{26}$–$B_{75}N_{75}H_{30}$	−4.77	−130.42	34.09	−102.54	−200.67	−42.74	−80.09	−175.72	−27.72	–
$C_{13}H_{28}$–$B_{75}N_{75}H_{30}$	−5.17	−142.35	37.25	−109.98	−212.71	−46.60	−86.18	−177.69	−33.23	–
$C_{14}H_{30}$–$B_{75}N_{75}H_{30}$	−5.54	−153.94	40.33	−116.57	−220.07	−50.99	−91.66	−192.97	−34.16	–

It can be seen that using the PM6 method without correction does not lead to any satisfactory results. In this case, $\Delta G_{298}^{bind} > 0$ indicating the disadvantage of the alkane binding with both types of adsorbents, which does not correspond to available experimental data [15,47,48]. The use of corrections of both types radically changes the calculation result: $\Delta G_{298}^{bind} < 0$ indicating possibility of alkane binding to the regarded surfaces. At the same time, the type of correction has almost no effect on the results of calculating the binding enthalpy of alkanes to tricircumcoronene, unlike to $B_{75}N_{75}H_{30}$. Thus, the contribution of one C–H$\cdots\pi$ interaction to ΔH_{298}^{bind} for alkanes on the surface of $B_{75}N_{75}H_{30}$ differs by about 25%–30% (1.6 kJ/mol) for the calculated values using DH2 and D3H4 corrections. In addition, the use of DH2 correction for alkane–$B_{75}N_{75}H_{30}$ complexes yields ΔH_{298}^{bind} values slightly higher than those for alkane–tricircumcoronene complexes, which contradicts experimental data on the isosteric adsorption heats of these compounds on the regarded adsorbent types [15,47], indicating a greater thermal effect upon adsorption on a carbon surface.

The calculation results are used to form correlation dependences for thermodynamic binding parameters in alkane–$C_{150}H_{30}$ and alkane–$B_{75}N_{75}H_{30}$ complexes of the form:

$$\Delta A_T^{bind} = (U_i^{bind} \pm \Delta U_i^{bind}) \cdot K_\pi + (V_i^{bind} \pm \Delta V_i^{bind}), \quad (6)$$

where ΔA_T^{bind} is the thermodynamic parameter of binding (enthalpy, entropy, Gibbs energy) of alkane molecule with $C_{150}H_{30}$ or $B_{75}N_{75}H_{30}$; the contributions of U_i^{bind} and V_i^{bind} depend on the considered thermodynamic characteristic, selected adsorbent, temperature (T = 298 K) and calculation method; K_π is the number of intermolecular C–H$\cdots\pi$ interactions between hydrogen atoms of CH_2 and CH_3 alkane fragments with aromatic rings of adsorbent (it is equal to the length of the alkane chain (n) provided its "parallel" orientation on the adsorbent surface). The coefficients of regression dependences are shown in Table 3.

Let us compare the obtained contributions of C–H$\cdots\pi$ interactions into ΔH_{298}^{bind} with experimental values and values estimated in the framework of the density functional theory B3LYP-D3/6-311G** (see Table S3 of the Supplementary Materials). Thus, the average increment of the isosteric heat of alkane adsorption on graphite per methylene fragment is 7.06 kJ/mol, and on hBN—5.60 kJ/mol according to the experimental data of studies [15,48], correspondingly. These values correlate quite well with the semi-empirical calculation data from the Table 3, as well as DFT calculations for short-chain alkane (C_2–C_4) complexes on coronene and its BNNS counterpart: −5.99 and −5.62 kJ/mol, respectively. For the case of alkanols (C_2–C_4) on coronene, the increment of C–H$\cdots\pi$ interaction into the binding energy amounts to −5.77 kJ/mol in PM6-DH2 and −5.92 kJ/mol in B3LYP-D4/6-311G**. Enlargement of the molecule, modelling the surface of adsorbent, leads

to the increase of the value of the mentioned increment to −6.40 and −7.81 kJ/mol on tricircumcoronene in PM6-D3H4 and PM6-DH2 correspondingly.

Table 3: Coefficients of linear dependences of the type $\Delta A_T^{bind} = (U_i^{bind} \pm U_i^{bind}) \cdot K_\pi + (V_i^{bind} \pm V_i^{bind})$ for binding thermodynamic characteristics in complexes alkane–$C_{150}H_{30}$ and alkane–$B_{75}N_{75}H_{30}$, R is correlarion coefficient, S is standard deviation.

System	Parameter	$U_i^{bind} \pm U_i^{bind}$	$V_i^{bind} \pm V_i^{bind}$	R	S
Alkane–$C_{150}H_{30}$ (in PM6-DH2 method)	ΔH_{298}^{bind}, kJ/mol	−7.62 ± 0.08	−7.54 ± 0.83	0.9996	0.62
	ΔS_{298}^{bind}, J/(mol·K)	−14.62 ± 0.94	−48.42 ± 9.73	0.9858	7.30
	ΔG_{298}^{bind}, kJ/mol	−3.26 ± 0.27	6.89 ± 2.79	0.9766	2.09
Alkane–$C_{150}H_{30}$ (in PM6-D3H4 method)	ΔH_{298}^{bind}, kJ/mol	−7.56 ± 0.06	−6.87 ± 0.58	0.9998	0.44
	ΔS_{298}^{bind}, J/(mol·K)	−9.47 ± 1.05	−55.17 ± 10.80	0.9599	8.10
	ΔG_{298}^{bind}, kJ/mol	−4.74 ± 0.27	9.57 ± 2.78	0.9889	2.08
Alkane–$B_{75}N_{75}H_{30}$ (in PM6-DH2 method)	ΔH_{298}^{bind}, kJ/mol	−8.01 ± 0.08	−6.30 ± 0.69	0.9995	1.05
	ΔS_{298}^{bind}, J/(mol·K)	−13.27 ± 0.52	−37.17 ± 4.60	0.9916	7.03
	ΔG_{298}^{bind}, kJ/mol	−4.06 ± 0.16	4.78 ± 1.44	0.9912	2.20
Alkane–$B_{75}N_{75}H_{30}$ (in PM6-D3H4 method)	ΔH_{298}^{bind}, kJ/mol	−6.30 ± 0.03	−4.41 ± 0.28	0.9999	0.43
	ΔS_{298}^{bind}, J/(mol·K)	−12.00 ± 0.27	−27.66 ± 2.43	0.9971	3.71
	ΔG_{298}^{bind}, kJ/mol	−2.72 ± 0.07	3.83 ± 0.58	0.9968	0.89

The contribution of C–H$\cdots\pi$ interactions to ΔS_{298}^{bind} exhibits a comparable variation in both systems when using either correction. Specifically, this difference amounts to approximately 30% for alkanes adsorbed on tricircumcoronene and nearly 20% for those on the boron nitride fragment. Consequently, an analysis of the key interaction contributions to alkane binding at the considered surfaces (as reflected in ΔG_{298}^{bind}) supports the recommendation to use the PM6-D3H4 method for further calculations of alkane film formation parameters on BNNS. In contrast, prior studies [19,20] on alkane film formation on graphene surfaces have demonstrated the adequacy of combining the DH2 correction with the PM6 method. This approach successfully reproduced the chain length of alkanes capable of spontaneous monolayer formation on graphite-like surfaces—14 carbon atoms in accordance with the experimental data obtained using STM [4,49,50] and AFM methods [51], X-ray diffraction analysis [6], as well as incoherent elastic neutron scattering [52]. The increments of C–H$\cdots\pi$ interaction into ΔG_{298}^{bind} derived from data calculated within DFT amounted to −4.19 and −3.73 kJ/mol for alkanes on $C_{24}H_{12}$ (coronene) and $B_{12}N_{12}H_{12}$ correspondingly, indicating less favorable interactions for the later. It is only 1 kJ/mole more than was assessed within semi-empirical PM6 method with corrections (see Table 3). The slightly lower preference of C–H$\cdots\pi$ interactions into ΔG_{298}^{bind} for alkanes on BNNS than on graphene (approximately 10%) gives rise to predict lower melting temperatures of alkane monolayers on BNNS than on graphene, which is recorded experimentally [15].

3.3 Thermodynamics of Crystalline Film Formation for C_nH_{2n+2} Alkanes (n = 6–14) on the BNNS Surface

To determine the thermodynamic parameters of alkane clusterization on the BNNS surface, the same methodological approach applied to alkane films on graphene [19] should be used. In addition to C–H$\cdots\pi$ interactions between the alkane and the polyaromatic system, it is essential to account for intermolecular interactions between alkane molecules in two possible directions of monolayer propagation (p and q). Differential scanning calorimetry studies of alkane melting on carbon-containing surfaces and hBN revealed

distinct features in the thermograms: (1) prominent peaks corresponding to the melting of the 3D phase; (2) barely discernible peaks attributed to 2D monolayers, which melt at higher temperatures [21]. The two small melting peaks for alkane monolayers on hBN differed by 1–2 K, interpreted by the authors as a pre-melting solid–solid phase transition. We propose that this phenomenon reflects a possible rearrangement of alkane molecules: after the 3D bulk alkane phase melts, a less stable monolayer forms and subsequently reorganizes into a more thermodynamically stable monolayer structure.

In this context, two possible packing types of alkane molecules in monolayers on isoelectronic surfaces (graphene and BNNS) are considered: "straight" and "herringbone". Fig. 4 illustrates fragments of such monolayers for BNNS, while analogous structures for graphene are shown in Fig. S1 of the Supplementary Materials. Alkane dimers are marked with dotted ovals; their intermolecular interactions should be considered when developing an additive scheme to evaluate the thermodynamics of film formation for the corresponding monolayers. The thermodynamic parameters of dimerization for isolated structures (without polyaromatic systems) are provided in Tables S4 and S5 of the Supplementary Materials.

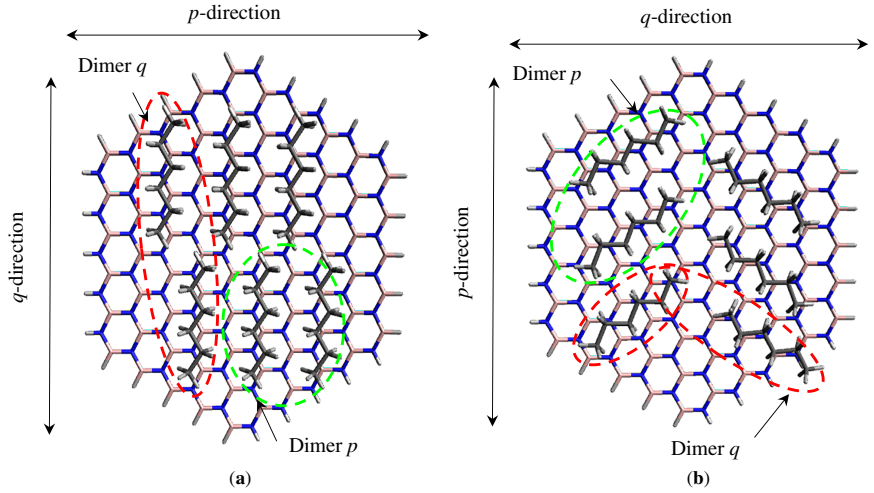

Figure 4: Fragments of 2D monolayer structure of alkanes on BNNS with "straight" (**a**) and "herringbone" (**b**) molecular packing (by the example of hexane–$B_{75}N_{75}H_{30}$ complex).

As already noted in previous study [19], the Gibbs energy of dimerization for all identified alkane dimer types exhibits subtle dependence on either the alkane chain length or the number of CH···HC interactions. This behavior stems from the fact that, in the *q* direction, alkane dimers involve only a single interaction between the terminal methyl groups of the alkane chains. Using the PM6-DH2 method, the average dimerization Gibbs energy for these associates is (16.37 ± 3.27) kJ/mol for the "straight" monolayer structure and (17.01 ± 1.33) kJ/mol for the "herringbone" structure; these values do not differ significantly within the computational uncertainty. The average values of ΔG_{298}^{dim} within the PM6-D3H4 method for the same dimer structures in the *q* direction are (15.92 ± 2.41) and (17.11 ± 1.86) kJ/mol for the "straight" and the "herringbone" monolayer, respectively, which is also indistinguishable, given the estimation errors.

The value of ΔG_{298}^{dim} is practically independent of the alkane chain length for dimers in the *p* direction due to the implementation of the energetically unfavorable "e" type of intermolecular CH···HC interactions, in contrast to the "a" type formed during the monolayer formation of substituted alkanes at the air/water interface [53]. The average Gibbs energy of dimerization of such clusters is (17.95 ± 1.20) and (19.58 ± 3.23) kJ/mol for the "straight" and the "herringbone" monolayers in PM6-DH2, and in PM6-D3H4 it was slightly lower, at the level of (17.10 ± 1.35) and (18.04 ± 1.71) kJ/mol, respectively.The coefficients of the

linear dependences ΔH_{298}^{dim} and ΔS_{298}^{dim} on the alkane chain length (n) in the PM6 method with two types of corrections are given in Table 4 for dimers formed in both directions of monolayer propagation:

$$\Delta A_T^{dim} = (U_i^{dim} \pm \Delta U_i^{dim}) \cdot n + (V_i^{dim} \pm \Delta V_i^{dim}), \quad (7)$$

where ΔA_T^{dim} is the thermodynamic dimerization parameter (enthalpy, entropy, or Gibbs energy) of alkanes; the contributions of U_i^{dim} and V_i^{dim} depend on the considered thermodynamic characteristic, the type of dimer, temperature (T = 298 K), and the calculation method; U_i^{dim} characterizes the contribution of CH···HC interactions between the methylene groups of alkanes, and V_i^{dim} is the contribution of interactions between the terminal methyl fragments of alkanes.

Table 4: Coefficients of linear dependences of the type $\Delta A_{298}^{dim} = (U_i^{dim} \pm \Delta U_i^{dim}) \cdot n + (V_i^{dim} \pm \Delta V_i^{dim})$ for thermodynamic dimerization parameters of alkanes, R is correlarion coefficient, S is standard deviation.

System	Parameter	$U_i^{dim} \pm \Delta U_i^{dim}$	$V_i^{dim} \pm \Delta V_i^{dim}$	R	S
For "straight" monolayer					
Dimer p (PM6-DH2)	ΔH_{298}^{dim}, kJ/mol	−2.45 ± 0.01	2.33 ± 0.14	0.9999	0.11
	ΔS_{298}^{dim}, J/(mol·K)	−7.40 ± 1.84	−65.28 ± 19.01	0.8352	14.26
Dimer p (PM6-D3H4)	ΔH_{298}^{dim}, kJ/mol	−3.04 ± 0.00	2.61 ± 0.01	1.0000	0.01
	ΔS_{298}^{dim}, J/(mol·K)	−11.11 ± 0.43	−42.48 ± 6.45	0.9948	3.34
Dimer q (PM6-DH2)	ΔH_{298}^{dim}, kJ/mol	–	−6.23 ± 0.01	–	–
	ΔS_{298}^{dim}, J/(mol·K)	–	−75.86 ± 11.00	–	–
Dimer q (PM6-D3H4)	ΔH_{298}^{dim}, kJ/mol	–	−1.90 ± 0.48	–	–
	ΔS_{298}^{dim}, J/(mol·K)	–	−59.82 ± 8.80	–	–
For "herringbone" monolayer					
Dimer p (PM6-DH2)	ΔH_{298}^{dim}, kJ/mol	−2.61 ± 0.11	6.49 ± 1.51	0.9964	0.46
	ΔS_{298}^{dim}, J/(mol·K)	−8.29 ± 0.87	−40.92 ± 9.97	0.9537	9.14
Dimer p (PM6-D3H4)	ΔH_{298}^{dim}, kJ/mol	−3.05 ± 0.09	4.88 ± 0.91	0.9971	0.68
	ΔS_{298}^{dim}, J/(mol·K)	−11.73 ± 0.83	−29.26 ± 8.62	0.9827	6.47
Dimer q (PM6-DH2)	ΔH_{298}^{dim}, kJ/mol	–	−3.74 ± 0.12	–	–
	ΔS_{298}^{dim}, J/(mol·K)	–	−69.53 ± 4.03	–	–
Dimer q (PM6-D3H4)	ΔH_{298}^{dim}, kJ/mol	–	−4.59 ± 0.17	–	–
	ΔS_{298}^{dim}, J/(mol·K)	–	−70.18 ± 4.70	–	–

Table 4 shows that interaction contributions in alkane dimers, calculated with semi-empirical corrections for dispersion and hydrogen bonding, do not differ significantly within the standard error except for the enthalpy of dimerization of Dimer q in the "straight" monolayer. Including both enthalpy and entropy factors yields ΔG_{298}^{dim} values that are nearly independent of chain length and the number of CH···HC interactions between alkane molecules.

The obtained energy contributions of interactions during the formation of alkane dimers, as well as interactions between alkanes and polyaromatic systems, make it possible to create the additive scheme. This scheme, in turn, enable to assess the possibility of alkanes to form 2D monolayers of various structures on the surface of BNNS and graphene at the given temperature and length of the alkane chain. Let's denote the numbers of contributions realized in the dimer structures in the p and q directions of the monolayer

propagation as n_p and n_q and define them as follows:

$$n_p = q \cdot (p-1),\ n_q = p \cdot (q-1), \tag{8}$$

where p and q are the numbers of alkane molecules in the corresponding directions of the monolayer propagation.

Intermolecular C–H$\cdots\pi$ interactions realize in both directions of the monolayer propagation. In this case, the dependence of their number on the length of the alkane hydrocarbon chain (n) can be determined as follows:

$$K_\pi = p \cdot q \cdot n. \tag{9}$$

In order to define the number of mentioned interactions per molecule of the infinite 2D cluster, it is necessary to divide the Eqs. (8) and (9) obtained above by the number of monomers in the cluster ($m = p{\cdot}q$), and then take the limit from these values as the number of molecules in the cluster tends to infinity. Then these dependences transform into the next:

$$n_{q,\infty}/m = n_{p,\infty}/m = 1. \tag{10}$$

It is possible to calculate the number of intermolecular C–H$\cdots\pi$ interactions per monomer in the 2D film according to the expression outlined below:

$$K_{\pi,\infty}/m = n. \tag{11}$$

Substitution of Eqs. (10) and (11) into Eq. (6), combined with the additives for dimer interaction from Eq. (7), yields an expression for the Gibbs clusterization energy per monomer in the 2D alkane film:

$$\Delta G^{Cl}_{298,\infty}/m = U_i^{Cl} \cdot n + V_i^{Cl}, \tag{12}$$

where the coefficients U_i^{Cl} and V_i^{Cl} are given in Table 5 for two considered types of monolayers on the isoelectronic surfaces of BNNS and graphene using the PM6 method with DH2 and D3H4 corrections.

Table 5: Coefficients of linear dependences for calculation of the Gibbs energy of 2D film formation per alkane molecule at standard temperature.

Method	Adsorbent	Parameter	
		U_i^{Cl}, kJ/mol	V_i^{Cl}, kJ/mol
For "straight" monolayer			
PM6-DH2	BNNS	−4.00	40.27
	Graphene	−3.26	42.43
PM6-D3H4	BNNS	−2.72	37.64
	Graphene	−4.74	43.44
For "herringbone" monolayer			
PM6-DH2	BNNS	−4.00	41.19
	Graphene	−3.26	43.48
PM6-D3H4	BNNS	−2.72	38,92
	Graphene	−4.74	44.72

STM, X-ray diffraction as well as incoherent elastic neutron scattering studies show that alkanes require at least 12–14 carbon atoms to form crystalline monolayers on carbon surfaces, and 14 atoms on hBN surfaces under standard conditions [4,6,21,49,51]. These values are consistent with the calculated results for alkanes on graphene using the PM6 method with DH2 correction, and for alkanes on BNNS—with D3H4 correction. It is illustrated in Fig. 5 showing the graphical representation of the obtained dependences $\Delta G^{Cl}_{298,\infty}/m$. The need to apply various corrections of the PM6 method can also be illustrated by the dependence of the temperature of spontaneous alkane film formation on the chain length, since it can be easily assessed using the expression for $\Delta G^{Cl}_{298,\infty}/m$ calculation.

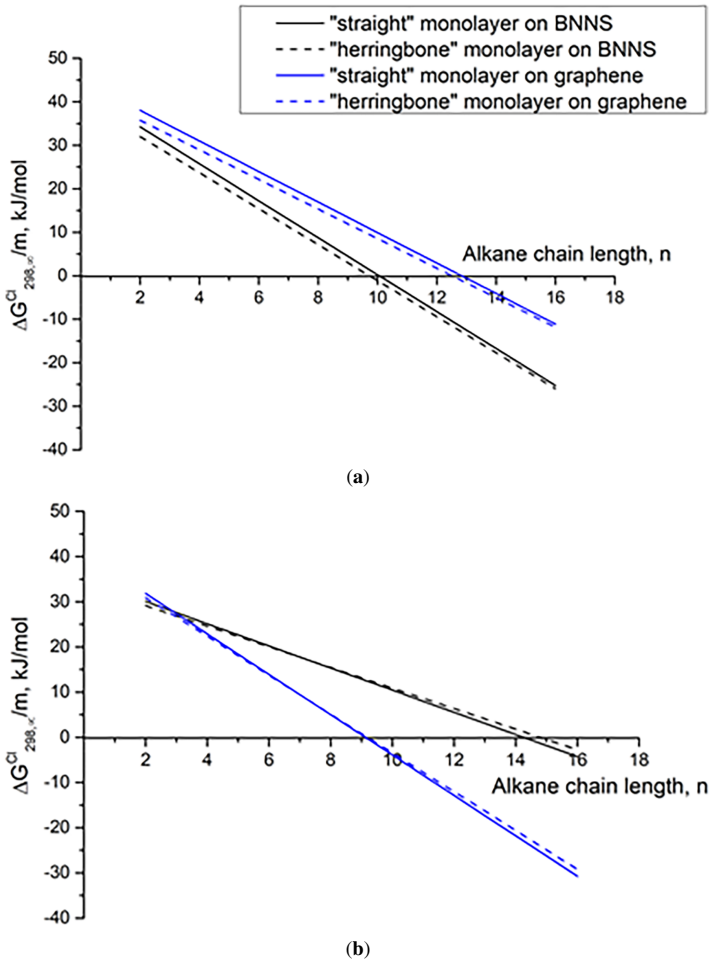

Figure 5: Dependences of clusterization Gibbs energy per alkane molecule of 2D monolayer assessed within PM6-DH2 (**a**) and PM6-D3H4 (**b**) at standard conditions.

Several schemes were previously developed for this purpose in study [54], differing in their degree of theoretical validity. These schemes were validated through assessments of the spontaneous film formation temperature for ten surfactant classes at the air/water interface. Particularly, even the most simplified scheme reproduces experimental data with a relatively low error of 3%–5%. Within the framework of the simplest scheme, the required temperature for spontaneous clusterization (or the melting temperature of the monolayer, T_m) can be estimated using the following expression:

$$T_m = \frac{\Delta H^{Cl}_{298,\infty}/m}{\Delta S^{Cl}_{298,\infty}/m}, \tag{13}$$

where the values $\Delta H^{Cl}_{298,\infty}/m$ and $\Delta S^{Cl}_{298,\infty}/m$ linearly depends on the number of C–H$\cdots\pi$ interactions ($K_{\pi,\infty}/m$), numerically equal to the length of the alkane chain (n). The film formation parameters can be expressed in terms of the corresponding thermodynamic parameters of alkane binding to the surface of adsorbents according to Eq. (6) and the parameters of alkane dimerization in the p and q directions of the monolayer propagation according to Eq. (7). Then Eq. (13) takes the form:

$$T_m = \frac{(U^{bind}_{\Delta H} + U^{dim}_{\Delta H,p} + U^{dim}_{\Delta H,q}) \cdot \mathrm{n} + V^{bind}_{\Delta H} + V^{dim}_{\Delta H,p} + V^{dim}_{\Delta H,q}}{(U^{bind}_{\Delta S} + U^{dim}_{\Delta S,p} + U^{dim}_{\Delta S,q}) \cdot \mathrm{n} + V^{bind}_{\Delta S} + V^{dim}_{\Delta S,p} + V^{dim}_{\Delta S,q}}. \tag{14}$$

The values of the corresponding coefficients U_i and V_i are given in Tables 3 and 4. The calculated values of the onset temperature of alkane spontaneous clusterization on 2D hexagonal boron nitride and graphene qualitatively reflect the experimental dependences [21], although with a systematic error, which increases with the elongation of the alkane chain (n):

$$\delta = (65.55 \pm 4.66) - (4.83 \pm 0.41)\mathrm{n} \qquad \text{for “straight” 2D monolayer on BNNS,} \tag{15}$$

$$\delta = (58.09 \pm 5.34) - (4.78 \pm 0.47)\mathrm{n} \qquad \text{for “straight” 2D monolayer on graphene-like surface.} \tag{16}$$

Accounting for this error significantly improves the agreement of calculated and experimental data on the onset temperature of 2D alkane film formation (Table S6 of Supplementary Materials). It should also be noted that the calculated temperature difference of spontaneous film formation for the “straight” monolayer and the “herringbone” monolayer, for instance, for dodecane is 1.9 K in excellent agreement with the experimentally recorded value of 2.0 K [21]. The authors of this work interpret it as pre-melting solid-solid phase transition. A similar behavior of dodecane has also been recorded during its melting on the surface of graphite [55]. While for the shorter-chain heptane, differential scanning calorimetry have shown no trace of molecular rearrangement in 2D monolayer preceding the melting of the bulk phase.

As demonstrated in Fig. 6, alkane films exhibit greater thermal stability on graphene surface compared to BNNS surface. Quantitative analysis reveals the following average relative differences between the melting temperatures of alkane monolayers and the corresponding 3D phase: 5% for even-chain alkanes, 9% for odd-chain alkanes on BNNS; 11% for even-chain alkanes, 14% for odd-chain alkanes on graphene. These computational results are in good agreement with experimental data reported by Arnold et al. [21], who observed: “on h-BN, the monolayer seems to melt at a temperature approximately 5% above the bulk melting point (for even chain length molecules) or 8% (for odd chain length molecules), compared with approximately 10% above the bulk (even) or 14% (odd) for alkanes on graphite”. This consistency confirms that C–H$\cdots\pi$ interactions between alkanes and solid surfaces contribute differently to monolayer stabilization, despite their isoelectricity. Particularly, C–H$\cdots\pi$ interactions on graphene are more energetically favorable than those on BN plane. To elucidate this difference, a detailed examination of the properties of benzene’s isoelectronic analogues where carbon atoms are replaced by boron and nitrogen is required.

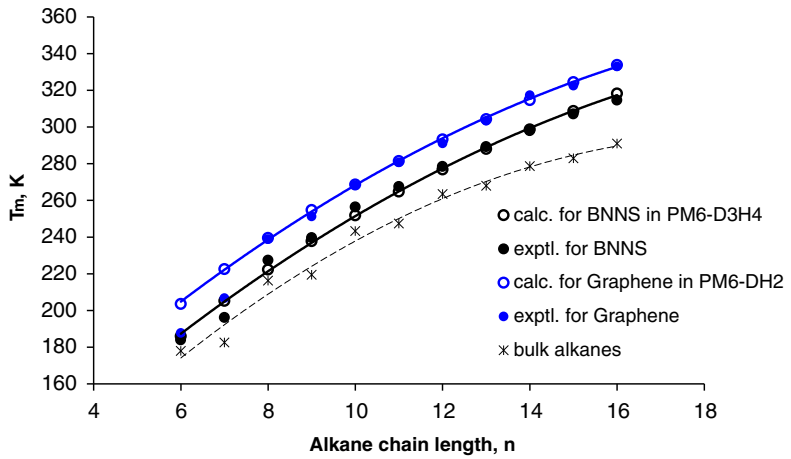

Figure 6: Dependences of the melting temperatures of 2D monolayers and the bulk phase of alkanes on the chain length on the surface BNNS (black line and circles) and graphene (blue line and circles). Lines just guide the eye.

Interactions between molecules with closed electron shells which are responsible for the processes of physisorption, film formation and crystallization realize mainly due to the dispersion forces. These include, in particular, CH···HC and C–H···π interactions. The experimental study [56], devoted to the charge density distribution of benzene, borazole and their halogenated derivatives, show that intermolecular interactions in the crystals of these compounds are also governed by the X–H···π (where X designates C, N or B atoms) and π···π interactions. Furthermore, as in benzene, these X–H···π interactions in borazole are controlled by the Pauli repulsion and the London dispersion. It is quite logical to associate the energy of such interactions between alkanes and aromatic compounds with the aromaticity of the solid surfaces, which differs despite their isoelectronics.

The aromaticity of borazole $B_3N_3H_6$, as the inorganic analog of benzene C_6H_6 and the structural element of BNNS, was recognized after rather long discussion [57–59]. Theoretical studies available in the literature and comparisons of the properties of these two molecules, as well as isoelectronic carborazole $C_2B_2N_2H_6$, have shown that all of them exhibit aromatic properties, however, decreasing in the series C_6H_6 > $C_2B_2N_2H_6$ > $B_3N_3H_6$. The lower aromaticity of other six-membered cycles containing boron and nitrogen atoms in different sequences is confirmed in Ref. [60]. In addition, studies of a number of BN-[n]helicenes have also confirmed their somewhat atypical aromaticity [61]. The calculation of the electron density of delocalized bonds ($EDDB_P$-π) performed by Wu et al. [57] showed that the π electrons are the best and equally delocalized on all carbon atoms in the benzene molecule. Boron atoms in carborazole and borazole have the least number of delocalized electrons compared to other atoms in the molecule. Thus, from the view point of the EDDB population analysis, boron atoms determine the lower limit of the entire electron delocalization, and, consequently, the aromaticity of the compared molecules.

Natural energy decomposition analysis for energy in the interaction of noble gas molecules with surfaces of graphene and BNNS [62] showed that contributions from the various terms follow the relative order: charge transfer > polarization > dispersion > exchange > electrostatic for the case of inert gas adsorption on BNNS. At the same time, major contribution to the attractive term comes from the dispersion term for the case of adsorption on graphene-like surfaces [62]. Therefore, based on this assumption, the lower energetic increment of C–H···π interactions between aliphatic chains and aromatic π-systems of graphene-like surfaces comparatively to hexagonal boron nitride surfaces is quite reasonable and proved by the experimental studies [15,21].

Finally, a detailed analysis of geometric parameters for *n*-alkane monolayer unit cells on BNNS (Fig. 7) and graphene (Fig. S2 in Supplementary Materials) reveals subtle but important peculiarities of alkane packing on regarded isoelectronic surfaces. Table 6 compiles data for "straight" and "herringbone" arrangements, validated against X-ray diffraction measurements [63]. For the "straight" structure on hBN, extrapolation from longer homologues ($C_{12}H_{26}$, $C_{14}H_{30}$, $C_{16}H_{34}$, [63]) shows a linear trend: the *b* side elongates by 5.35 Å per two methylene units, while the *a* side remains fixed at 4.32 Å. Therefore, the data presented for the longer side *b* of the hexane unit cell are obtained by extrapolation. In "herringbone" structures, the angle φ between molecular axes for lamellas differs slightly: 120° on BNNS vs. 122° on graphene. These values align well with experimental data for alkanes and their substituted ones [18,64], confirming the accuracy of the optimized models. In general, the systematical larger unit cell dimensions on hBN are observed by ~2% increase in interplanar lattice constant: 2.52 Å vs. graphite's 2.46 Å.

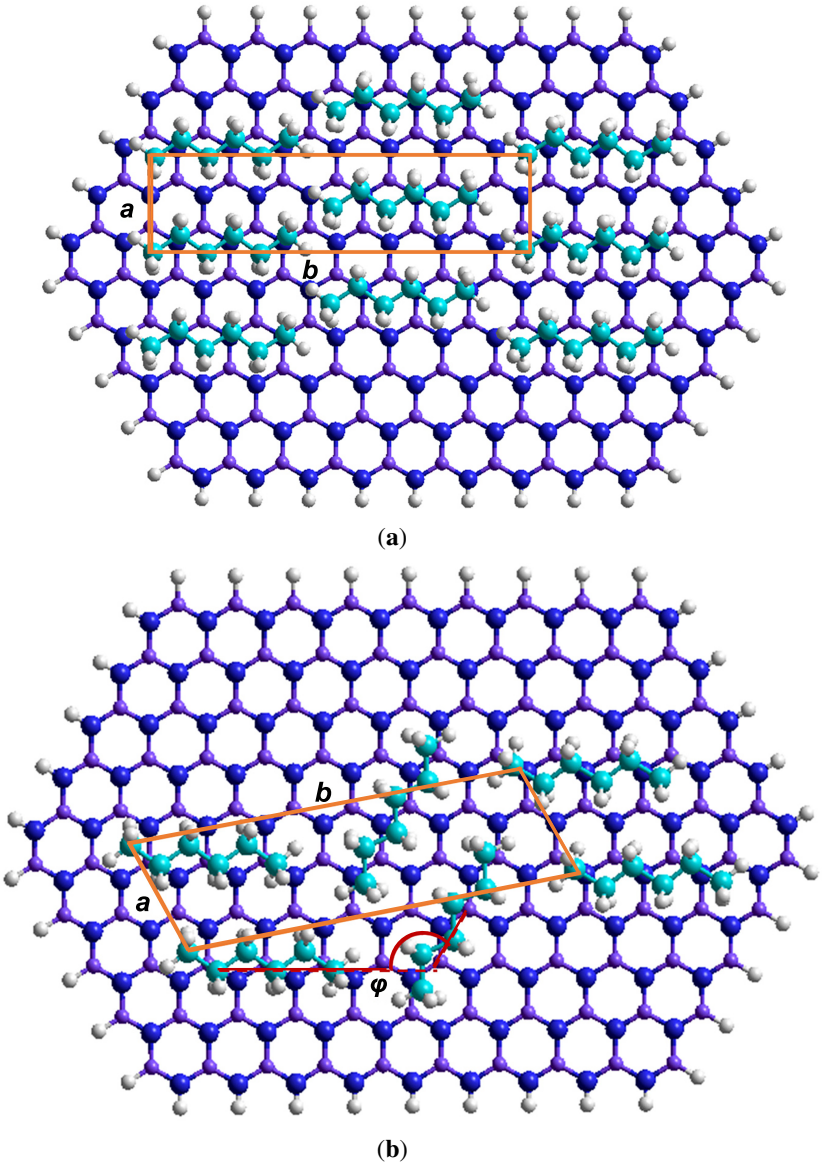

Figure 7: Illustration of geometrical parameters of the unit cell for 2D monolayer structures of alkanes on BNNS with "straight" (**a**) and "herringbone" (**b**) molecular packing.

Table 6: Parameters of 2D unit cells for alkane monolayers on isoelectronic surfaces.

Monolayer Structure	BNNS		Graphene	
	Calc. PM6-D3H4	Exptl. [63]	Calc. PM6-DH2	Exptl. [63,65]
"Straight"	(4.41 × 19.07) Å	(4.32 × 18.25) Å*	(4.28 × 17.44) Å	(4.92 × 17.04) Å
"Herringbone"	(5.15 × 17.01) Å	(5.01 × 17.15) Å	(5.08 × 16.94) Å	(4.90 × 16.90) Å

Note: *extrapolated for C_6H_{14} using data for $C_{12}H_{26}$, $C_{14}H_{30}$, $C_{16}H_{34}$ in Ref. [63].

4 Conclusions

This study reports quantum chemical semi-empirical calculations of thermodynamic and structural parameters for 2D alkane film formation on isoelectronic adsorbents: BNNS and graphene. The performed calculations showed that:

(1) accurate PM6-based modelling of "hydrocarbon–model surface molecule" systems requires dispersion interactions and hydrogen bond corrections as their contributions are crucial for the intermolecular C–H$\cdots\pi$ interactions occurring in such systems. In the case of alkane binding to the BNNS surface, the D3H4 correction should be applied, while the DH2 correction is more adequate for the case of graphene surface, when comparing experimentally estimated values of adsorption heats.

(2) C–H$\cdots\pi$ interaction contributions to alkane binding are ~20% lower on BNNS than on graphene, due to the lower aromaticity of borazole ring compared to benzene as structural elements of the corresponding isoelectronic adsorbents.

(3) the threshold chain lengths of alkanes capable of forming crystalline monolayers on the surface of BNNS and graphene differ by one methylene fragment and amount to 14 and 13 carbon atoms, respectively.

(4) there are two possible types of alkane molecule packing during their 2D monolayer formation on the chosen surfaces: the so-called "straight" and "herringbone" monolayers. In terms of Gibbs clusterization energy, these monolayer structures are similar, with a slightly lower preference for the "herringbone" monolayer for longer hydrocarbons on the BNNS surface. The possible existence of two types of alkane monolayers can be interpreted as pre-melting solid-solid phase transition.

(5) the dependence of the temperature of spontaneous alkane film formation on the chain length is estimated for two solid surfaces. The calculated temperature difference between spontaneous film formation of the "straight" and "herringbone" monolayer for dodecane is 1.9 K, in agreement with the experimentally recorded value of 2.0 K.

The obtained results are of interest in the theoretical justification of the experimental data available in the literature. It is valuable due to the lack of micrographs for the structure of alkane adsorption layers on the hBN surface, because of the dielectric properties of boron nitride and the inability to conduct STM studies, as well as the neutron absorption property of $_{10}B$ isotope, hindering the neutron scattering studies.

Acknowledgement: Not applicable.

Funding Statement: This research was funded by Ministry of Science and Higher Education of the Russian Federation within state budget assignment "Preparation and analysis of supramolecular and doped carbon structures with industrially useful properties (FRES-2026-0015)".

Availability of Data and Materials: The data that support the findings of this study are available within the Article or Supplementary Materials.

Ethics Approval: Not applicable.

Conflicts of Interest: The author declares no conflicts of interest.

Supplementary Materials: The supplementary material is available online at https://www.techscience.com/doi/10.32604/cmc.2026.082702/s1. Table S1: Structural parameters borazole molecule calculated within different methods; Table S2: Thermodynamic parameters of formation for alkanes, benzene, borazole, tricircumcoronene and $B_{75}N_{75}H_{30}$ in gaseous phase within semi-empirical methods; Table S3: Binding thermodynamic parameters for short-chain alkanes with molecules modelling the surface of BNNS and graphene; Table S4: Thermodynamic parameters of alkane dimerization within PM6-DH2 method; Table S5: Thermodynamic parameters of alkane dimerization within PM6-D3H4 method; Figure S1: Fragment of 2D monolayer structure of alkanes on graphene with "straight" (a) and "herringbone" (b) molecular packing (by the example of hexane–$C_{150}H_{30}$ complex); Table S6: Melting temperature for alkane 2D monolayer on isoelectronic surfaces and 3D bulk phase; Figure S2: Illustration of geometrical parameters of the unit cell for 2D monolayer structures of alkanes on graphene with "straight" (a) and "herringbone" (b) molecular packing.

References

1. Avgul NN, Berezin GI, Kiselev AV, Lygina IA. Energy of adsorption forces and heat of adsorption of n-alkanes on graphitized carbon black. Russ Chem Bull. 1957;6(9):1052–61. doi:10.1007/BF01169381.
2. Avgul NN, Berezin GI, Kiselev AV, Lygina IA. The adsorption and heat of adsorption of normal alcohols on graphitized carbon black. Russ Chem Bull. 1961;10(2):186–93. doi:10.1007/BF00919549.
3. Ilan B, Florio GM, Hybertsen MS, Berne BJ, Flynn GW. Scanning tunneling microscopy images of alkane derivatives on graphite: role of electronic effects. Nano Lett. 2008;8(10):3160–5. doi:10.1021/nl8014186.
4. Zhao M, Jiang P, Deng K, Yu AF, Hao YZ, Xie SS, et al. Insight into STM image contrast of n-tetradecane and n-hexadecane molecules on highly oriented pyrolytic graphite. Appl Surf Sci. 2011;257(8):3243–7. doi:10.1016/j.apsusc.2010.10.150.
5. Giancarlo LC, Flynn GW. Scanning tunneling and atomic force microscopy probes of self-assembled, physisorbed monolayers: peeking at the peaks. Annu Rev Phys Chem. 1998;49(1):297–336. doi:10.1146/annurev.physchem.49.1.297.
6. Espeau P, Reynolds PA, Dowling T, Cookson D, White JW. X-ray diffraction from layers of n-alkanes adsorbed on graphite. Faraday Trans. 1997;93(17):3201–8. doi:10.1039/a701071k.
7. Morishige K, Kato T. Chain-length dependence of melting of *n*-alcohol monolayers adsorbed on graphite: n-hexanol, *n*-heptanol, *n*-octanol, and *n*-nonanol. J Chem Phys. 1999;111(15):7095–102. doi:10.1063/1.480001.
8. Novoselov KS, Jiang D, Schedin F, Booth TJ, Khotkevich VV, Morozov SV, et al. Two-dimensional atomic crystals. Proc Natl Acad Sci U S A. 2005;102(30):10451–3. doi:10.1073/pnas.0502848102.
9. Urade AR, Lahiri I, Suresh KS. Graphene properties, synthesis and applications: a review. JOM. 2023;75(3):614–30. doi:10.1007/s11837-022-05505-8.
10. Zhu PJ, Yan YN, Zhou Y, Qi ZJ, Li YF, Chen CM. Thermal properties of graphene and graphene-based nanocomposites: a review. ACS Appl Nano Mater. 2024;7(8):8445–63. doi:10.1021/acsanm.4c00411.
11. Hess P. Group IIIA–VA monolayers. In: Bonding, structure, and performance of two-dimensional materials: an introduction based on the periodic table. Cham, Switzerland: Springer; 2025. p. 153–90.
12. Wahida F, Larese JZ. Adsorption of cyclopentane on MgO(100), hexagonal boron nitride, and graphite basal planes: a thermodynamic and modeling study. J Phys Chem C. 2018;122(44):25301–13. doi:10.1021/acs.jpcc.8b06487.
13. Kamaraj M, Sundar JV, Subramanian V. Dioxin sensing properties of graphene and hexagonal boron nitride based van der Waals solids: a first-principles study. RSC Adv. 2016;6(108):107114–26. doi:10.1039/c6ra18976h.
14. Bahrami E, Barenji AD, Khabazi ME, Chermahini AN. Boron nitride nanosheets: a comprehensive review of synthesis and multifunctional applications. Results Chem. 2025;17:102655. doi:10.1016/j.rechem.2025.102655.
15. Strange N, Larese JZ. High-resolution volumetric adsorption and molecular dynamics of the *n*-alkanes on the surface of hexagonal boron nitride. J Phys Chem C. 2018;122(37):21308–21. doi:10.1021/acs.jpcc.8b04278.

16. Gordeev EG, Polynski MV, Ananikov VP. Fast and accurate computational modeling of adsorption on graphene: a dispersion interaction challenge. Phys Chem Chem Phys. 2013;15(43):18815–21. doi:10.1039/c3cp53189a.
17. Kikkawa Y, Tsuzuki S. Stability of *n*-alkanes and *n*-perfluoroalkanes against horizontal displacement on a graphite surface. Phys Chem Chem Phys. 2024;26(37):24314–21. doi:10.1039/d4cp02418d.
18. Morishige K, Takami Y, Yokota Y. Structures of alkanes and alkanols adsorbed on graphite in solution: comparison with scanning-tunneling-microscopy images. Phys Rev B. 1993;48(11):8277–81. doi:10.1103/physrevb.48.8277.
19. Kartashynska ES. Quantum chemical modeling of alkane 2D monolayer formation on graphene. JCIS Open. 2024;15:100117. doi:10.1016/j.jciso.2024.100117.
20. Kartashynska ES. Thermodynamics and structure of 2D aliphatic alcohol monolayers on graphene within semi-empirical quantum chemical approach. Theor Chem Acc. 2025;144(4):25. doi:10.1007/s00214-025-03181-w.
21. Arnold T, Parker JE, Macdonald P. Investigation of the adsorption of alkanes on hexagonal boron nitride from their liquids and binary mixtures. J Phys Chem C. 2012;116(19):10599–606. doi:10.1021/jp300649a.
22. Forster M, Parker JE, Inaba A, Murray CA, Strange NA, Larese JZ, et al. The mixing behavior of alkanes adsorbed on hexagonal boron nitride. J Phys Chem C. 2016;120(45):25796–805. doi:10.1021/acs.jpcc.6b07701.
23. Hughes TJ, Shaw RA, Russo SP. Computational investigations of dispersion interactions between small molecules and graphene-like flakes. J Phys Chem A. 2020;124(46):9552–61. doi:10.1021/acs.jpca.0c06595.
24. Smith DG, Patkowski K. Interactions between methane and polycyclic aromatic hydrocarbons: a high accuracy benchmark study. J Chem Theory Comput. 2013;9(1):370–89. doi:10.1021/ct3008809.
25. Kikkawa Y, Tsuzuki S. Interaction energies and stabilities of heteroatom-containing aromatic compounds on graphite. Phys Chem Chem Phys. 2026;28(11):7093–100. doi:10.1039/d5cp04566e.
26. Bin Yeamin M, Faginas-Lago N, Albertí M, Cuesta IG, Sánchez-Marín J, Sánchez de Merás AMJ. Multi-scale theoretical investigation of molecular hydrogen adsorption over graphene: coronene as a case study. RSC Adv. 2014;4(97):54447–53. doi:10.1039/c4ra08487j.
27. John C, Swathi RS. An anisotropic dressed pairwise potential model for the adsorption of noble gases on boron nitride sheets. Phys Chem Chem Phys. 2022;24(4):2554–66. doi:10.1039/d1cp04815e.
28. Mason SE, Beton PH, Besley NA. AIRBED: a simplified density functional theory model for physisorption on surfaces. J Chem Theory Comput. 2019;15(10):5628–34. doi:10.1021/acs.jctc.9b00576.
29. Yadav A, Dindorkar SS. Adsorption behaviour of hexagonal boron nitride nanosheets towards cationic, anionic and neutral dyes: insights from first principle studies. Colloids Surf A Physicochem Eng Aspects. 2022;640:128509. doi:10.1016/j.colsurfa.2022.128509.
30. Saha B, Bhattacharyya PK. Density functional study on the adsorption of 5-membered N-heterocycles on B/N/BN-doped graphene: coronene as a model system. ACS Omega. 2018;3(12):16753–68. doi:10.1021/acsomega.8b02340.
31. Yin S, Wang C, Qiu X, Xu B, Bai C. Theoretical study of the effects of intermolecular interactions in self-assembled long-chain alkanes adsorbed on graphite surface. Surf Interface Anal. 2001;32(1):248–52. doi:10.1002/sia.1047.
32. McGonigal GC, Bernhardt RH, Thomson DJ. Imaging alkane layers at the liquid/graphite interface with the scanning tunneling microscope. Appl Phys Lett. 1990;57(1):28–30. doi:10.1063/1.104234.
33. Couto MS, Liu XY, Meekes H, Bennema P. Scanning tunneling microscopy studies on *n*-alkane molecules adsorbed on graphite. J Appl Phys. 1994;75(1):627–9. doi:10.1063/1.355799.
34. Vysotsky YB, Bryantsev VS, Fainerman VB, Vollhardt D, Miller R. Quantum chemical analysis of thermodynamics of the two-dimensional cluster formation at the air/water interface. J Phys Chem B. 2002;106(1):121–31. doi:10.1021/jp012919q.
35. Kartashynska ES, Vollhardt D. Description of surfactant 2D monolayer formation at the air/water interface within semiempirical quantum chemistry. JCIS Open. 2024;14(2):100110. doi:10.1016/j.jciso.2024.100110.
36. Stewart JJP. MOPAC2016, version: 19.168W. [cited 2025 Jan 1]. Available from: http://OpenMOPAC.net.
37. Neese F. Software update: the ORCA program system—version 5.0. WIREs Comput Mol Sci. 2022;12(5):e1606. doi:10.1002/wcms.1606.
38. Boys SF, Bernardi F. The calculation of small molecular interactions by the differences of separate total energies. Some procedures with reduced errors. Mol Phys. 1970;19(4):553–66. doi:10.1080/00268977000101561.

39. Haque S, Rahman MA, Islam MAM, Hossain A. Computational insights into the electronic, chemical, and thermodynamic properties of borazine and its derivatives. Results Chem. 2025;17:102634. doi:10.1016/j.rechem.2025.102634.
40. Nelson RD Jr, Lide DR Jr, Maryott AA. Selected values of electric dipole moments for molecules in the gas phase. Washington, DC, USA: American National Bureau of Standards; 1967.
41. Tsuzuki S, Fujii A. Nature and physical origin of CH/π interaction: significant difference from conventional hydrogen bonds. Phys Chem Chem Phys. 2008;10(19):2584. doi:10.1039/b718656h.
42. Karthikeyan S, Ramanathan V, Mishra BK. Influence of the substituents on the CH...π interaction: benzene–methane complex. J Phys Chem A. 2013;117(30):6687–94. doi:10.1021/jp404972f.
43. Tsuzuki S, Honda K, Uchimaru T, Mikami M, Tanabe K. The magnitude of the CH/π interaction between benzene and some model hydrocarbons. J Am Chem Soc. 2000;122(15):3746–53. doi:10.1021/ja993972j.
44. Shibasaki K, Fujii A, Mikami N, Tsuzuki S. Magnitude of the CH/π interaction in the gas phase: experimental and theoretical determination of the accurate interaction energy in benzene-methane. J Phys Chem A. 2006;110(13):4397–404. doi:10.1021/jp0605909.
45. Meyer EA, Castellano RK, Diederich F. Interactions with aromatic rings in chemical and biological recognition. Angew Chem Int Ed. 2003;42(11):1210–50. doi:10.1002/anie.200390319.
46. Paytakov G, Dinadayalane T, Leszczynski J. Toward selection of efficient density functionals for van der Waals molecular complexes: comparative study of C–H$\cdots\pi$ and N–H$\cdots\pi$ interactions. J Phys Chem A. 2015;119(7):1190–200. doi:10.1021/jp511450u.
47. Lal M, Spencer D. Interaction of alkanes with graphite. J Chem Soc Faraday Trans 2. 1974;70:910. doi:10.1039/f29747000910.
48. Isirikyan AA, Kiselev AV. The absolute adsorption isotherms of vapors of nitrogen, benzene and n-hexane, and the heats of adsorption of benzene and n-hexane on graphitized carbon blacks. I. Graphitized thermal blacks. J Phys Chem. 1961;65(4):601–7. doi:10.1021/j100822a004.
49. Chen Q, Yan HJ, Yan CJ, Pan GB, Wan LJ, Wen GY, et al. STM investigation of the dependence of alkane and alkane ($C_{18}H_{38}$, $C_{19}H_{40}$) derivatives self-assembly on molecular chemical structure on HOPG surface. Surf Sci. 2008;602(6):1256–66. doi:10.1016/j.susc.2008.01.030.
50. Wang D, Wan LJ, Bai CL. Formation and structural transition of molecular self-assembly on solid surface investigated by scanning tunneling microscopy. Mater Sci Eng R Rep. 2010;70(3–6):169–87. doi:10.1016/j.mser.2010.06.016.
51. Gosvami NN, O'Shea SJ. Nanoscale trapping and squeeze-out of confined alkane monolayers. Langmuir. 2015;31(47):12960–7. doi:10.1021/acs.langmuir.5b03133.
52. Castro MA, Clarke SM, Inaba A, Thomas RK. Solid monolayers adsorbed at the solid-liquid interface studied by incoherent elastic neutron scattering. J Phys Chem B. 1997;101(44):8878–82. doi:10.1021/jp9713221.
53. Vysotsky YB, Belyaeva EA, Fainerman VB, Aksenenko EV, Vollhardt D, Miller R. Quantum chemical analysis of the thermodynamics of 2-dimensional cluster formation of alkylamines at the air/water interface. J Phys Chem C. 2007;111(42):15342–9. doi:10.1021/jp074615v.
54. Vysotsky YB, Fomina ES, Belyaeva EA, Vollhardt D, Fainerman VB, Miller R. Temperature effect on the monolayer formation of substituted alkanes at the air/water interface: a quantum chemical approach. J Phys Chem B. 2012;116(30):8996–9006. doi:10.1021/jp303617n.
55. Arnold T, Thomas RK, Castro MA, Clarke SM, Messe L, Inaba A. The crystalline structures of the even alkanes hexane, octane, decane, dodecane and tetradecane monolayers adsorbed on graphite at submonolayer coverages and from the liquid. Phys Chem Chem Phys. 2002;4(2):345–51. doi:10.1039/B108190J.
56. Merino-García MDR, Soriano-Agueda LA, Guzmán-Hernández JD, Martínez-Otero D, Landeros Rivera B, Cortés-Guzmán F, et al. Benzene and borazine, so different, yet so similar: insight from experimental charge density analysis. Inorg Chem. 2022;61(18):6785–98. doi:10.1021/acs.inorgchem.1c03923.
57. Wu Y, Yan X, Liu Z, Lu T, Zhao M, Xu J, et al. Aromaticity in isoelectronic analogues of benzene, carborazine and borazine, from electronic structure and magnetic property. Chem Eur J. 2024;30(66):e202403369. doi:10.1002/chem.202403369.

58. Boese R, Maulitz AH, Stellberg P. Solid-state borazine: does it deserve to be entiteled “inorganic benzene”? Chem Ber. 1994;127(10):1887–9. doi:10.1002/cber.19941271011.
59. Báez-Grez R, Pino-Rios R. The hidden aromaticity in borazine. RSC Adv. 2022;12(13):7906–10. doi:10.1039/d1ra06457f.
60. Imran S, Gao Y, Wang W, Zhu J. Charge-driven stability and aromaticity of $C_2N_2B_2H_4$ isomers: insights from a combined DFT and machine learning study. Org Biomol Chem. 2025;23(18):4508–18. doi:10.1039/d5ob00131e.
61. Liu X, Xie X, Jin Z, Zhang X, Shen C. A DFT study on boron-nitrogen helicenes. Comput Theor Chem. 2023;1230:114396. doi:10.1016/j.comptc.2023.114396.
62. Ambrosetti A, Silvestrelli PL. Adsorption of rare-gas atoms and water on graphite and graphene by van der Waals-corrected density functional theory. J Phys Chem C. 2011;115(9):3695–702. doi:10.1021/jp110669p.
63. Arnold T, Forster M, Athanasiou Fragkoulis A, Parker JE. Structure of normal-alkanes adsorbed on hexagonal-boron nitride. J Phys Chem C. 2014;118(5):2418–28. doi:10.1021/jp4063059.
64. Yang T, Berber S, Liu JF, Miller GP, Tománek D. Self-assembly of long chain alkanes and their derivatives on graphite. J Chem Phys. 2008;128(12):124709. doi:10.1063/1.2841478.
65. Feng H, Becker KE, Zhou J, Fichthorn KA. Molecular thin films on solid surfaces: mechanisms of melting. Langmuir. 2012;28(19):7382–92. doi:10.1021/la300826p.